Dose coefficients for ICRP reference pediatric phantoms exposed to idealised external gamma fields

IOP Publishing | Society for Radiological Protection Journal of Radiological Protection
J. Radiol. Prot. 37 (2017) 127–144 (18pp) doi:10.1088/1361-6498/aa559e

Dose coefficients for ICRP reference pediatric phantoms exposed to idealised external gamma fields

Lienard A Chang[1], Steven L Simon[1], Timothy J Jorgensen[2], David A Schauer[3] and Choonsik Lee[1]

[1] Radiation Epidemiology Branch, Division of Cancer Epidemiology and Genetics, National Cancer Institute, National Institutes of Health, Rockville, MD 20850, United States
[2] Department of Radiation Medicine, Georgetown University, Washington, DC 20057, United States
[3] International Commission on Radiation Units and Measurements (ICRU), Bethesda, MD 20814, United States

E-mail: choonsik.lee@nih.gov

Received 10 May 2016, revised 20 December 2016
Accepted for publication 23 December 2016
Published 24 January 2017

Abstract

Organ and effective dose coefficients have been calculated for the International Commission on Radiological Protection (ICRP) reference pediatric phantoms externally exposed to mono-energetic photon radiation (x- and gamma-rays) from 0.01 to 20 MeV. Calculations used Monte Carlo radiation transport techniques. Organ dose coefficients, i.e., organ absorbed dose per unit air kerma (Gy/Gy), were calculated for 28 organs and tissues including the active marrow (or red bone marrow) for 10 phantoms (newborn, 1 year, 5 year, 10 year, and 15 year old male and female). Radiation exposure was simulated for 33 photon mono-energies (0.01–20 MeV) in six irradiation geometries: antero-posterior (AP), postero-anterior, right lateral, left lateral, rotational, and isotropic. Organ dose coefficients for different ages closely agree in AP geometry as illustrated by a small coefficient of variation (COV) (the ratio of the standard deviation to the mean) of 4.4% for the lungs. The small COVs shown for the effective dose and AP irradiation geometry reflect that most of the radiosensitive organs are located in the front part of the human body. In contrast, we observed differences in organ dose coefficients across the ages of the phantoms for lateral irradiation geometries. We also observed variation in dose coefficients across different irradiation geometries, where the COV ranges from 18% (newborn male) to 38% (15 year old male) across idealised whole body irradiation geometries for the major organs (active marrow, colon, lung, stomach wall, and breast) at the energy of 0.1 MeV.

Effective dose coefficients were also derived for applicable situations, e.g., radiation protection or risk projection. Our results are the first comprehensive set of organ and effective dose coefficients applicable to children and adolescents based on the newly adopted ICRP pediatric phantom series. Our tabulated organ and effective dose coefficients for these next-generation phantoms should provide more accurate estimates of organ doses in children than earlier dosimetric models allowed.

Supplementary material for this article is available online

Keywords: external photon, Monte Carlo radiation transport, organ dose, children

(Some figures may appear in colour only in the online journal)

1. Introduction

Assessing organ doses to members of the public from external radiation exposure is important because radiation-related health risk varies by organ site. Increasing number of studies suggested that radiation risks could be much greater for infants and children compared to adults [1] although newer findings report that differences might be lower than previously believed [2]. Potential radiation exposures to the general public include exposure to medical radiation procedures (both diagnostic and therapeutic), natural background radiation, exposure from nuclear power generation or accident, consumer products that use radioactive materials and possibly terrorist attacks involving dirty bombs.

The absorbed dose to any organ tissues of the human body is not directly measurable from radiation exposure. One must convert measurable physical quantities, such as air kerma or fluence, to organ absorbed dose by using dose coefficients [3–5]. To determine dose coefficients, computational human phantoms representing human anatomy are generally coupled with a Monte Carlo computer simulation code. The earliest phantoms were known as stylised (or mathematical) phantoms, in which the contours of body and organs were described by mathematical equations [6]. Those phantoms offered flexibility for modification but were not anatomically realistic. The next generation, voxel (volume element) or tomographic phantoms, were created from medical images, mostly computed tomography (CT) or magnetic resonance (MR) images and provide superior anatomical realism [7, 8]. However, due to the constraints of voxels, it is time-consuming to modify the phantom and organ sizes, shapes, and locations. The newest generation of phantoms is known as hybrid (or boundary representation) phantoms, which combine the advantages of both the stylised and voxel phantoms and are both flexible and anatomically realistic [7].

The International Commission on Radiological Protection (ICRP) introduced reference adult male and female voxel phantoms in ICRP Publication 110 [9]. Since ICRP 21 [10] in 1973, the ICRP has released three reports with a tabulation of organ and effective dose coefficients for external radiation: ICRP Publication 51 [3], ICRP Publication 74 [4], and ICRP Publication 116 [5]. The dose coefficients in those volumes focused on adults, emphasising radiation protection of workers. Previously, the dose calculations were made using hermaphrodite or sex-specific stylised phantoms [3, 4, 10]; for ICRP Publication 116 [5], the most recent report published by ICRP on reference dose coefficients, the values were calculated using the adult male and female voxel ICRP reference computational phantoms [9].

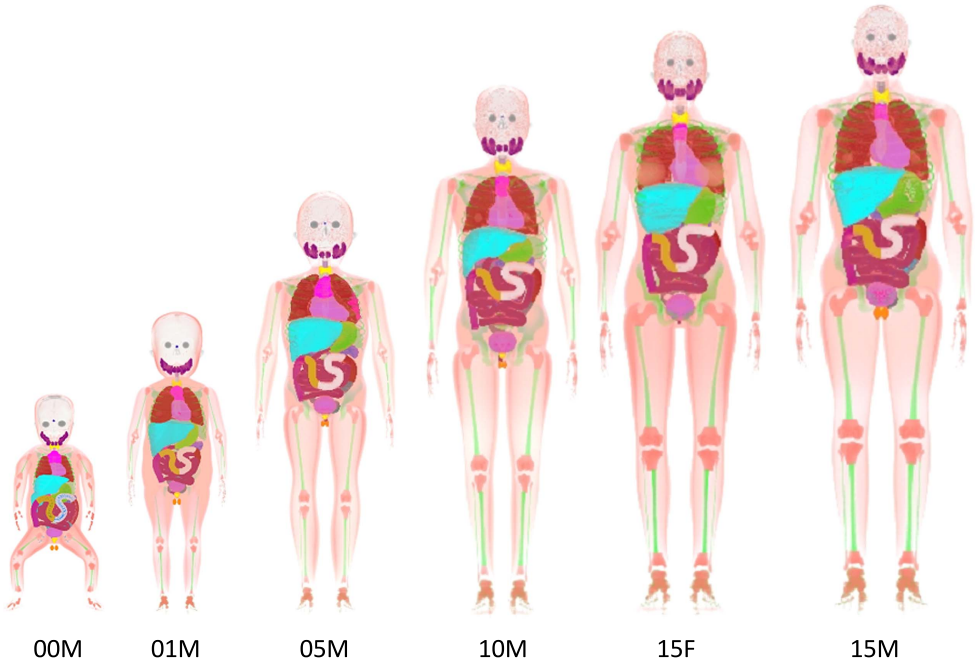

Figure 1. Frontal views of the ICRP pediatric phantom series representing newborn male (00M), 1 year old male (01M), 5 year old male (05M), 10 year old male (10M), and 15 year old female (15F) and male (15M) reference individuals.

Several papers have been published concerning dose coefficients for children and adolescents. Yamaguchi reported age-dependent effective dose coefficients for external photon radiation [11] and neutrons [12] based on the pediatric stylised phantom series developed at Oak Ridge National Laboratory (ORNL). Chou *et al* also used the ORNL phantom series to calculate dose coefficients for external photon radiation [13] and neutrons [14] over extensive energy ranges. The first voxel pediatric phantoms [15] were developed by German Research Center for Environmental Health (HMGU) (formerly GSF) and utilised in dosimetry for internal radiation sources [16], environmental exposure [15, 17–19], and medical radiation exposures [20–23]. The HMGU voxel phantoms were then followed by Caon *et al* [24]. Lee *et al* [25] reported dose coefficients for external photon radiation based on both the ORNL stylised phantoms and a series of pediatric voxel phantoms [26]. In some cases, these authors observed significant dose errors introduced by the unrealistic anatomy of the stylised phantoms.

After the introduction of the reference adult voxel phantoms, the ICRP adopted the voxel format of the hybrid pediatric phantom series [27] developed at the University of Florida and National Cancer Institute. The current work presents a comprehensive set of organ and effective dose coefficients for children and adolescents based on the newly adopted ICRP pediatric phantom series.

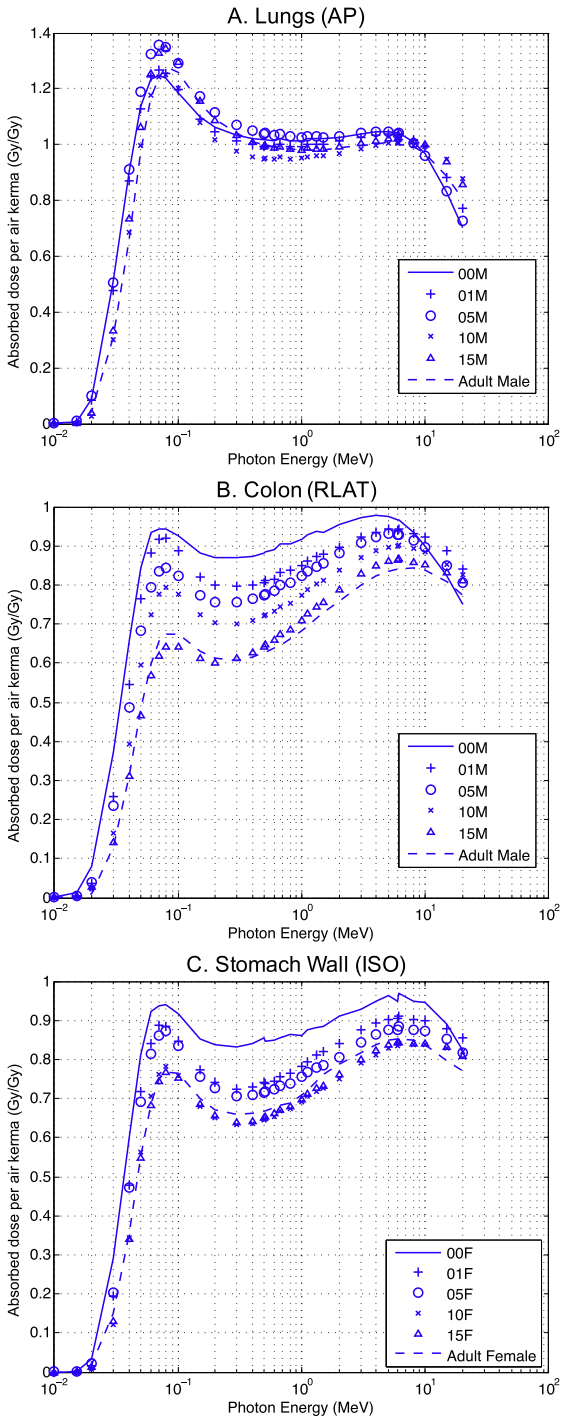

Figure 2. Dependency of dose coefficients on the age of the phantoms for (a) the lungs in AP geometry, (b) the colon in RLAT geometry, and (c) the stomach wall in ISO geometry. The data from the ICRP reference adult phantoms (ICRP Publication 116) is also included for comparison.

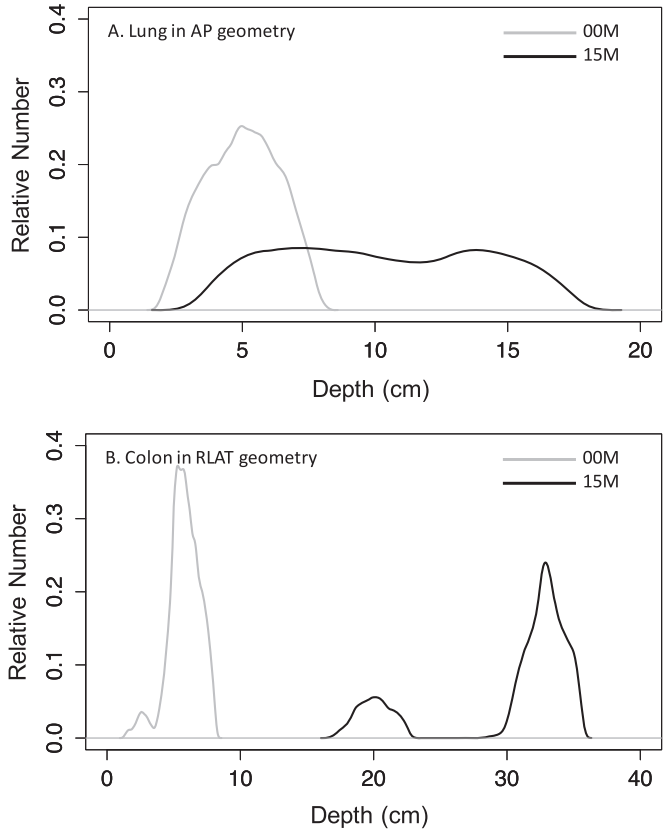

Figure 3. Distribution of the depth from the body surface to (a) the lungs in AP geometry and (b) the colon in RLAT geometry for the newborn and 15 year old phantoms.

2. Materials and methods

2.1. Computational human phantoms

We used a series of reference pediatric phantoms consisting of a total of 10 voxel phantoms representing newborn, 1, 5, 10, and 15 year old males and females as shown in figure 1. The voxel phantoms were developed by using the original hybrid phantoms as templates [27], which were based on polygon mesh and non-uniform rational B-spline surfaces. Each age-dependent hybrid phantom was developed from respective CT image set of a patient close to the respective age with organs manually contoured, which were then adjusted to match the reference organ mass published in ICRP Publication 89 [28]. The anatomies of the male and female phantoms from newborn to 10 year old is identical except for the gonads and urinary bladders. The list of organs and tissues and their ID of the hybrid phantom series were modified to comply with the ICRP reference adult phantoms [9]. Several additional tissues including oral mucosa, sub-structures in the breast, lung blood, ureters, and skeletal muscles were additionally modelled in the ICRP paediatric phantoms. Each phantom has a total of 139 organs and tissues defined including cortical and spongiosa bones. The voxel size for the phantoms varies with age, ranging from $2.9 \times 10^{-4}\,\mathrm{cm}^3$ for the newborn to $4.4 \times 10^{-3}\,\mathrm{cm}^3$

for the phantom of the 15 year old male. Age-dependent elemental composition and density are adopted from ICRP Publication 89 [28] and International Commission on Radiation Units and Measurements (ICRU) Report 46 [29], which is consistent with the ICRP reference adult phantoms.

2.2. Calculation of dose coefficients

Dose coefficients, which are the ratio of organ absorbed dose (Gy) to air kerma (Gy), were calculated for 28 organs and tissues, 33 mono photon energies (0.01–20 MeV), and six different irradiation geometries: antero-posterior (AP), postero-anterior (PA), right and left lateral (RLAT/LLAT), rotational (ROT), and isotropic (ISO). The organs and tissues required for effective dose calculation [30] were selected for the current study: adrenals, brain, breasts, colon, esophagus, extrathoracic, gall bladder wall, heart wall, kidney, lens, liver, lungs, lymph nodes, muscle, oral mucosa, ovaries, pancreas, prostate, salivary glands, small intestine wall, skin, spleen, stomach wall, testes, thymus, thyroid, urinary bladder wall, and uterus. To calculate active (or red bone marrow) and shallow (or bone surface) bone marrow, we scored the fluence passing the spongiosa structure of different bone sites including cranium, mandible, scapulae, clavicles, sternum, ribs, cervical, thoracic, and lumbar vertebrae, sacrum, os coxae, femora, patellae, ankle, feet, humera, radii, ulnae, and hands. For the 28 organs, energy deposition (MeV) was calculated to derive the organ absorbed dose (Gy).

Computer simulation was conducted using a general-purpose Monte Carlo radiation transport code, MCNPX 2.7 [31]. We followed the same approach taken in ICRP Publication 116 [5] underscoring the importance of tracking secondary electrons, which was not conducted in ICRP Publication 74 [4] where the kerma approximation was assumed. While the kerma approximation significantly decreases computer run time, it yields inaccuracies for thin or walled organs and tissues (e.g., skin) at photon energies above 1 MeV. The energy deposition tally of MCNPX2.7 allows for the calculation of absorbed dose (equation (1)) and subsequently dose conversion coefficient (equation (2)).

$$D\ (\mathrm{Gy}) = \frac{E\ (\mathrm{MeV}) \times 1.602 \times 10^{-13}\left(\frac{\mathrm{J}}{\mathrm{MeV}}\right)}{\mathrm{Organ\ Mass\ (kg)}}, \tag{1}$$

$$\mathrm{Dose\ \ coefficient}\left(\frac{\mathrm{Gy}}{\mathrm{Gy}}\right) = \frac{D\ (\mathrm{Gy})}{K\ (\mathrm{Gy})} = \frac{D\ (\mathrm{Gy})}{\mathrm{FKC}(\mathrm{pGy} \times \mathrm{cm}^2) \times \frac{1}{10^6}\left(\frac{\mathrm{Gy}}{\mathrm{pGy}}\right)} \times A\ (\mathrm{cm}^2), \tag{2}$$

where FKC is fluence-to-kerma conversion coefficients [4] and A is the area of the photon surface source.

For the active and shallow bone marrow dose coefficients, the photon fluence (photons m^{-2}) was scored at the 19 different bone sites mentioned above. The resulting output was used in conjunction with the fluence-to-dose response functions (DRF) (mGy m^2), originally tabulated by Eckerman *et al* [32] and later updated by Johnson *et al* [33]. The description of this method can be found in ICRP Publication 116 [5]. The DRFs allow for conversion of fluence into an absorbed dose deposited in the trabecular structures at each bone site. The age-dependent distribution of active and shallow bone marrow [28] was then used to derive bone site-average dose coefficients for active and shallow marrows, respectively. Effective dose coefficients were computed from the equivalent doses calculated for organs of the reference male and female of the respective age, as defined in ICRP Publication 103 [30].

For both the organ and the skeletal dose coefficients, a total of 5.0×10^8 photon particles were simulated for every combination of the 10 phantoms, 33 photon energy bins, and six

Table 1. (a) Effective dose coefficients (Sv/Gy) for the reference (a) newborn, (b) 1 year old, (c) 5 year old, (d) 10 year old, and (e) 15 year old exposed to external photons with energy bins from 0.01 to 20 MeV in the AP, PA, RLAT, LLAT, ROT, and ISO irradiation geometries.

(a) Newborn	Effective dose coefficients (Sv/Gy)					
Energy (MeV)	AP	PA	RLAT	LLAT	ROT	ISO
0.01	2.1E-02	4.6E-03	4.0E-03	3.9E-03	7.8E-03	6.3E-03
0.015	0.104	0.029	0.032	0.032	0.050	0.043
0.02	0.237	0.097	0.085	0.092	0.138	0.115
0.03	0.624	0.414	0.316	0.348	0.449	0.366
0.04	0.966	0.763	0.582	0.630	0.773	0.653
0.05	1.182	0.997	0.773	0.823	0.988	0.836
0.06	1.273	1.107	0.874	0.926	1.103	0.918
0.07	1.290	1.129	0.901	0.950	1.128	0.947
0.08	1.284	1.152	0.914	0.957	1.104	0.950
0.1	1.237	1.105	0.899	0.944	1.090	0.926
0.15	1.149	1.035	0.856	0.898	1.024	0.872
0.2	1.101	1.005	0.843	0.880	0.985	0.861
0.3	1.057	0.976	0.841	0.869	0.959	0.859
0.4	1.033	0.966	0.842	0.870	0.956	0.847
0.5	1.021	0.967	0.853	0.877	0.945	0.851
0.511	1.025	0.972	0.854	0.881	0.958	0.849
0.6	1.017	0.968	0.856	0.881	0.951	0.846
0.662	1.023	0.975	0.874	0.892	0.967	0.860
0.8	1.014	0.963	0.872	0.895	0.957	0.854
1	1.010	0.975	0.880	0.900	0.947	0.872
1.117	1.014	0.976	0.888	0.907	0.982	0.886
1.33	1.010	0.971	0.894	0.911	0.969	0.890
1.5	1.003	0.973	0.900	0.913	0.961	0.883
2	0.974	0.978	0.910	0.924	0.944	0.913
3	0.935	0.972	0.909	0.919	0.937	0.900
4	0.898	0.969	0.902	0.914	0.920	0.903
5	0.870	0.958	0.894	0.902	0.899	0.881
6	0.839	0.938	0.877	0.890	0.889	0.864
6.129	0.839	0.941	0.877	0.887	0.892	0.874
8	0.782	0.906	0.845	0.857	0.849	0.838
10	0.729	0.873	0.823	0.822	0.811	0.799
15	0.609	0.776	0.758	0.751	0.727	0.737
20	0.503	0.686	0.700	0.683	0.635	0.674

(b) 1 year old	Effective dose coefficients (Sv/Gy)					
Energy (MeV)	AP	PA	RLAT	LLAT	ROT	ISO
0.01	1.5E-02	2.3E-03	2.7E-03	2.7E-03	5.4E-03	4.3E-03
0.015	0.078	0.011	0.021	0.021	0.034	0.030
0.02	0.177	0.054	0.063	0.062	0.094	0.078
0.03	0.515	0.317	0.253	0.268	0.357	0.283
0.04	0.875	0.661	0.514	0.545	0.679	0.542
0.05	1.136	0.923	0.728	0.767	0.922	0.743

Table 1. (Continued.)

(b) 1 year old	Effective dose coefficients (Sv/Gy)					
Energy (MeV)	AP	PA	RLAT	LLAT	ROT	ISO
0.06	1.271	1.070	0.852	0.890	1.062	0.862
0.07	1.306	1.118	0.897	0.936	1.108	0.900
0.08	1.310	1.126	0.911	0.948	1.118	0.915
0.1	1.255	1.089	0.891	0.922	1.075	0.886
0.15	1.142	1.005	0.836	0.863	0.993	0.831
0.2	1.086	0.964	0.813	0.837	0.954	0.805
0.3	1.035	0.938	0.804	0.825	0.923	0.788
0.4	1.012	0.929	0.807	0.827	0.914	0.784
0.5	0.998	0.926	0.811	0.831	0.909	0.787
0.511	1.000	0.928	0.815	0.833	0.911	0.790
0.6	0.993	0.925	0.820	0.837	0.908	0.790
0.662	0.999	0.933	0.830	0.846	0.912	0.798
0.8	0.991	0.931	0.833	0.851	0.913	0.809
1	0.988	0.934	0.846	0.862	0.921	0.815
1.117	0.993	0.941	0.856	0.872	0.920	0.823
1.33	0.989	0.942	0.864	0.878	0.926	0.835
1.5	0.985	0.945	0.869	0.883	0.926	0.843
2	0.974	0.952	0.883	0.896	0.938	0.852
3	0.935	0.959	0.894	0.904	0.932	0.868
4	0.903	0.957	0.892	0.901	0.919	0.866
5	0.879	0.954	0.885	0.894	0.911	0.861
6	0.856	0.944	0.875	0.881	0.892	0.847
6.129	0.858	0.946	0.876	0.883	0.892	0.850
8	0.816	0.921	0.849	0.855	0.862	0.830
10	0.786	0.902	0.825	0.834	0.839	0.806
15	0.701	0.844	0.779	0.786	0.777	0.761
20	0.621	0.779	0.739	0.742	0.720	0.717

(c) 5 year old	Effective dose coefficients (Sv/Gy)					
Energy (MeV)	AP	PA	RLAT	LLAT	ROT	ISO
0.01	9.7E-03	2.0E-03	1.8E-03	2.0E-03	3.6E-03	2.9E-03
0.015	0.074	0.008	0.017	0.019	0.031	0.026
0.02	0.192	0.043	0.054	0.060	0.092	0.075
0.03	0.546	0.270	0.195	0.226	0.328	0.261
0.04	0.921	0.589	0.393	0.445	0.624	0.493
0.05	1.197	0.852	0.573	0.634	0.862	0.690
0.06	1.345	1.008	0.687	0.751	1.005	0.806
0.07	1.392	1.069	0.737	0.802	1.061	0.857
0.08	1.399	1.089	0.758	0.821	1.074	0.871
0.1	1.344	1.065	0.757	0.812	1.049	0.860
0.15	1.222	0.990	0.725	0.773	0.973	0.803
0.2	1.157	0.951	0.712	0.756	0.936	0.779
0.3	1.098	0.923	0.713	0.752	0.906	0.762
0.4	1.067	0.917	0.722	0.757	0.897	0.765
0.5	1.049	0.911	0.732	0.765	0.893	0.767

Table 1. (Continued.)

(c) 5 year old	Effective dose coefficients (Sv/Gy)					
Energy (MeV)	AP	PA	RLAT	LLAT	ROT	ISO
0.511	1.051	0.915	0.735	0.769	0.895	0.770
0.6	1.040	0.912	0.743	0.773	0.895	0.775
0.662	1.043	0.920	0.756	0.787	0.901	0.785
0.8	1.027	0.920	0.764	0.792	0.901	0.793
1	1.021	0.922	0.781	0.807	0.907	0.803
1.117	1.024	0.929	0.794	0.818	0.915	0.812
1.33	1.019	0.930	0.806	0.828	0.921	0.821
1.5	1.015	0.932	0.813	0.835	0.920	0.830
2	1.011	0.945	0.837	0.859	0.933	0.849
3	0.981	0.956	0.865	0.881	0.939	0.864
4	0.952	0.964	0.877	0.892	0.933	0.868
5	0.924	0.965	0.880	0.893	0.928	0.869
6	0.894	0.964	0.878	0.888	0.917	0.861
6.129	0.895	0.966	0.881	0.889	0.919	0.865
8	0.846	0.951	0.864	0.871	0.891	0.846
10	0.807	0.941	0.851	0.859	0.870	0.829
15	0.723	0.903	0.822	0.825	0.826	0.798
20	0.651	0.856	0.800	0.797	0.781	0.765

(d) 10 year old	Effective dose coefficients (Sv/Gy)					
Energy (MeV)	AP	PA	RLAT	LLAT	ROT	ISO
0.01	6.3E-03	1.8E-03	1.7E-03	1.7E-03	2.9E-03	2.4E-03
0.015	0.056	0.005	0.016	0.017	0.026	0.023
0.02	0.146	0.022	0.046	0.048	0.073	0.062
0.03	0.439	0.174	0.155	0.173	0.252	0.204
0.04	0.792	0.443	0.331	0.368	0.516	0.411
0.05	1.082	0.701	0.506	0.555	0.750	0.599
0.06	1.254	0.874	0.628	0.679	0.904	0.727
0.07	1.319	0.955	0.689	0.741	0.973	0.783
0.08	1.337	0.988	0.717	0.769	0.999	0.808
0.1	1.291	0.979	0.723	0.768	0.987	0.799
0.15	1.171	0.912	0.692	0.731	0.914	0.750
0.2	1.106	0.875	0.678	0.713	0.878	0.725
0.3	1.045	0.851	0.679	0.708	0.848	0.711
0.4	1.016	0.845	0.687	0.714	0.842	0.713
0.5	1.000	0.844	0.696	0.722	0.842	0.715
0.511	1.001	0.846	0.699	0.725	0.844	0.718
0.6	0.990	0.846	0.708	0.732	0.843	0.722
0.662	0.995	0.856	0.720	0.745	0.852	0.733
0.8	0.983	0.856	0.728	0.752	0.851	0.740
1	0.978	0.863	0.746	0.767	0.858	0.752
1.117	0.982	0.875	0.760	0.781	0.868	0.764
1.33	0.979	0.880	0.773	0.793	0.873	0.775
1.5	0.978	0.885	0.783	0.801	0.877	0.779

Table 1. (Continued.)

(d) 10 year old Energy (MeV)	Effective dose coefficients (Sv/Gy)					
	AP	PA	RLAT	LLAT	ROT	ISO
2	0.979	0.899	0.811	0.826	0.889	0.803
3	0.964	0.920	0.843	0.856	0.909	0.828
4	0.940	0.931	0.856	0.865	0.908	0.837
5	0.917	0.936	0.859	0.870	0.903	0.840
6	0.895	0.935	0.854	0.863	0.895	0.835
6.129	0.895	0.938	0.857	0.865	0.896	0.839
8	0.855	0.928	0.840	0.848	0.872	0.817
10	0.826	0.924	0.829	0.837	0.860	0.810
15	0.765	0.907	0.809	0.814	0.827	0.787
20	0.711	0.886	0.794	0.796	0.797	0.767

(e) 15 year old Energy (MeV)	Effective dose coefficients (Sv/Gy)					
	AP	PA	RLAT	LLAT	ROT	ISO
0.01	3.7E-03	1.7E-03	1.2E-03	1.4E-03	1.9E-03	1.5E-03
0.015	0.041	0.005	0.010	0.012	0.017	0.014
0.02	0.127	0.016	0.034	0.041	0.057	0.047
0.03	0.422	0.132	0.128	0.159	0.220	0.176
0.04	0.780	0.368	0.273	0.328	0.458	0.364
0.05	1.080	0.617	0.420	0.492	0.684	0.544
0.06	1.268	0.794	0.527	0.606	0.838	0.669
0.07	1.344	0.886	0.585	0.664	0.913	0.729
0.08	1.369	0.931	0.615	0.694	0.946	0.759
0.1	1.332	0.936	0.627	0.698	0.941	0.759
0.15	1.208	0.881	0.606	0.667	0.878	0.715
0.2	1.137	0.847	0.596	0.652	0.843	0.691
0.3	1.071	0.825	0.599	0.650	0.817	0.678
0.4	1.038	0.821	0.610	0.658	0.810	0.679
0.5	1.017	0.821	0.623	0.667	0.808	0.683
0.511	1.019	0.824	0.626	0.670	0.811	0.686
0.6	1.006	0.826	0.635	0.678	0.812	0.690
0.662	1.010	0.835	0.648	0.690	0.821	0.701
0.8	0.996	0.836	0.660	0.699	0.821	0.706
1	0.989	0.845	0.680	0.718	0.831	0.720
1.117	0.993	0.854	0.695	0.731	0.840	0.733
1.33	0.987	0.861	0.712	0.744	0.847	0.745
1.5	0.985	0.866	0.723	0.755	0.852	0.752
2	0.988	0.884	0.754	0.784	0.871	0.776
3	0.987	0.905	0.796	0.820	0.893	0.808
4	0.975	0.917	0.819	0.840	0.902	0.825
5	0.957	0.925	0.831	0.849	0.903	0.832
6	0.937	0.925	0.832	0.849	0.896	0.830
6.129	0.937	0.928	0.835	0.851	0.897	0.832
8	0.892	0.918	0.826	0.839	0.878	0.820
10	0.859	0.915	0.820	0.830	0.864	0.811
15	0.785	0.905	0.801	0.808	0.831	0.789
20	0.724	0.890	0.785	0.787	0.804	0.768

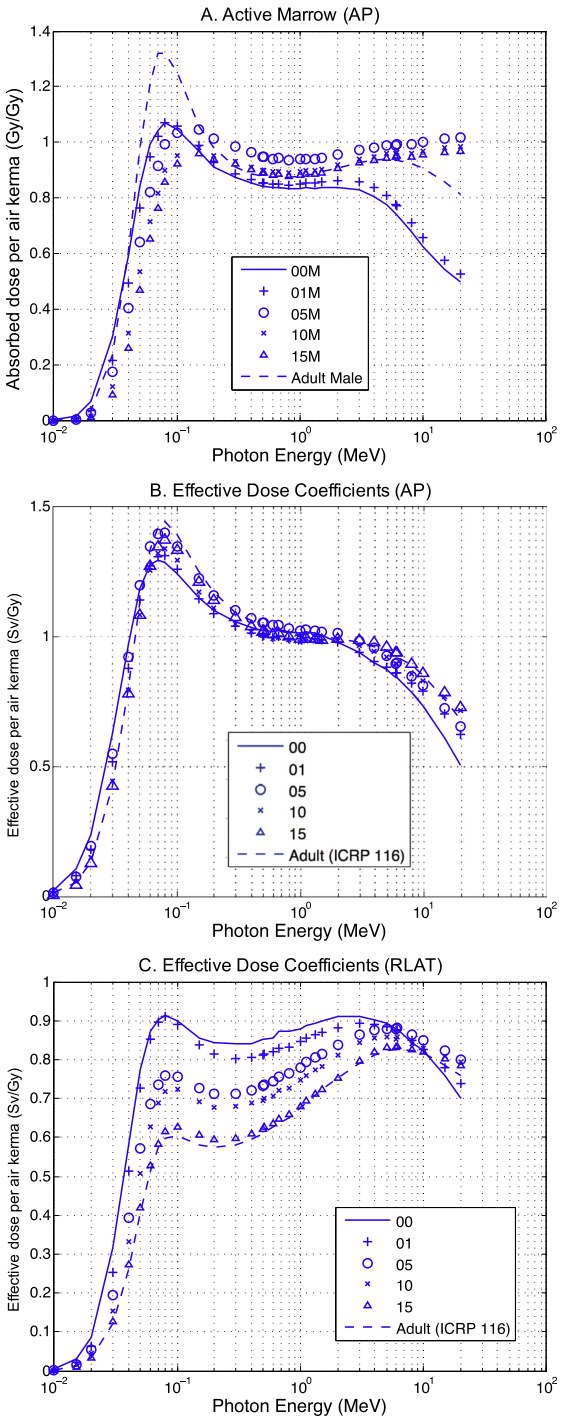

Figure 4. Dependency of (a) the active marrow dose coefficients in AP geometry, (b) effective dose coefficients in AP geometry, and (c) effective dose coefficients in RLAT geometry on the age of the phantoms. The data from the ICRP reference adult phantoms (ICRP Publication 116) is also included for comparison.

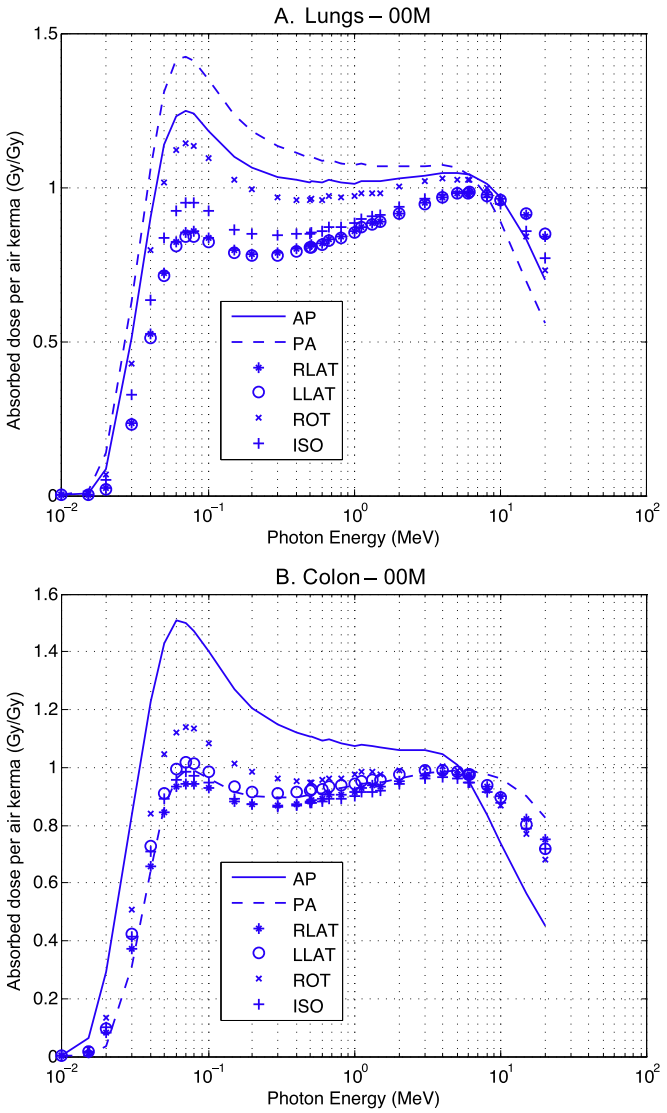

Figure 5. Dependency of organ dose coefficients on different irradiation geometries for (a) the lungs and (b) the colon of the newborn male phantom.

irradiation geometries, which generated a total of 1980 MCNPX input files. We confirmed that the relative error from Monte Carlo calculations was less than 1% for major organs in all irradiation geometries and for the energy of photons greater than 0.1 MeV. However, it must be noted that the relative errors were greater than 1% for the small organs (e.g., pituitary gland) for the energies lower than 0.1 MeV.

To expedite the calculations, a 50 keV secondary electron cutoff energy was used. The simulations were run on a 24-core MacBook Pro server as well as the National Institute of Health's Biowulf cluster, a GNU/Linux parallel processing system. Total run-time was approximately two months. MATLAB (MathWorks, Inc. Natwick, MA) scripts were written

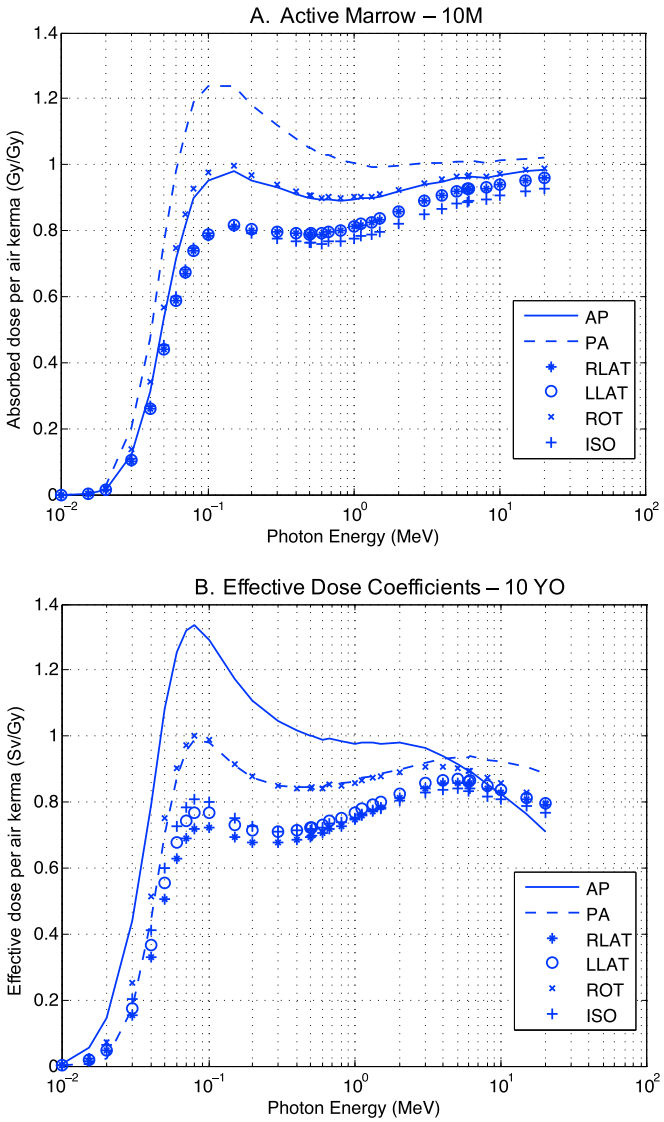

Figure 6. Dependency of (a) the active marrow and (b) effective dose coefficients on irradiation geometries for the 10 year old phantoms.

to automatically generate the input files for Monte Carlo simulations and to process the output files from MCNPX2.7 to calculate organ and effective dose coefficients.

3. Results and discussion

3.1. Comprehensive dose coefficients for pediatric phantoms

Organ dose coefficients, i.e. organ absorbed dose per air kerma (Gy/Gy), and effective dose coefficients (Sv/Gy) were tabulated for every combination of phantom, 28 organs and 2 skeletal tissues, 6 irradiation geometries, and 33 photon energies. Effective dose coefficients

for 6 irradiation geometries are tabulated in table 1. Complete tables for all organs in ten phantoms can be found in the supplementary data file. The change in organ dose coefficients with energy is relatively consistent between organs for the same irradiation geometry. At photon energies above 0.01 MeV, there is a lower photoelectric effect as well as an increased amount of Compton scattering, leading to relatively greater organ dose coefficient values. This trend continues until the dose coefficient reaches its peak around 0.06–0.1 MeV where photons reach their highest scattering angles. Above 10 MeV, the dose coefficient begins to plateau and decreases, which is mainly due to secondary electron escape from the organs becoming more prominent. These observations are in agreement with those reported in the ICRP Publication 74 [4] and 116 [5].

3.2. Dependency of dose coefficients on age

Figure 2 presents, as examples, the organ dose coefficients as a function of photon energy for (a) the lungs in AP geometry, (b) the colon in RLAT geometry, and (c) the stomach wall in ISO geometry of the phantoms with different ages. Because most of the major organs are located towards the front of the human body, we did not observe significant difference in organ dose coefficients across the ages of the phantoms in the AP irradiation geometry. As shown in figure 2(a), the dose coefficients for lungs of the five phantoms of different ages range from 1.184 to 1.294 Gy/Gy at 0.1 MeV with a small variation by age, coefficient of variation (COV, the ratio of the standard deviation to the mean) of 4.4%. In contrast, we observed large variation by age in dose coefficients for the colon for RLAT geometry as shown in figure 2(b). Photons incident from the lateral direction experience more shielding due to the adipose and muscle tissues in large phantoms than in small phantoms: 0.642 Gy/Gy and 0.962 Gy/Gy at 0.1 MeV in the 15 year old male and newborn male phantoms, respectively, with the COV of 13.6% across the phantoms of different ages. We also included the data for adult male from ICRP Publication 116 [5] for comparison. In both irradiation geometries, AP and RLAT, the data for adult male do not show significant difference from those of the 15 year old male phantom. We observed the COV of 8.2% in dose coefficients at 0.1 MeV for the stomach wall in the female phantoms in ISO geometry as shown in figure 2(c) which is still greater degree of variation than that of the lungs in AP geometry.

To further investigate the dependency of organ dose coefficients on age for AP and RLAT geometries, we calculated the distribution of the depth of a location randomly sampled within the lung and colon of the newborn and 15 year old male phantoms from the body surface (e.g., the frontal end of voxel phantoms in case of AP geometry), which are depicted in figure 3. The method to derive the depth distribution is the same one used for Annex E of ICRP Publication 110 [9]. Figure 3(a) shows the distribution of the depth for the lung in AP geometry for the newborn and 15 year old male phantoms. Although the 15 year old phantom shows a wider spread of the depth distribution (2–19 cm) due to having a thicker torso than the newborn, the depth distribution nearly overlaps with that of the newborn (2–9 cm). Radiation in AP geometry will penetrate a similar depth of soft tissue to reach the lungs, which explains the minimal discrepancy in dose coefficients in AP geometry (figure 2(a)). However, as shown in figure 3(b), the depth distribution of the colon in the 15 year old phantom (17–36 cm) is completely separated from that of the newborn phantom (1–8 cm). Radiation in RLAT geometry must penetrate more than 16 cm greater depth to reach the colons in the 15 year old phantom than the newborn.

Figure 4(a) shows the calculated dose coefficients for active marrow in AP irradiation geometry for different ages. As shown in figure 2(a) for the lungs in AP geometry, no substantial difference in active marrow doses was observed between the newborn and the 15

year old phantoms: 0.924–1.056 Gy/Gy with a COV of 5.9%. At higher energies (greater than 1 MeV), the active marrow dose coefficients for the newborn and 1 year old phantoms begin to decrease. We hypothesise that the high energy radiation hardly interacts with the very thin spongiosa region in the newborn and 1 year old phantoms so that dose coefficients become smaller as the photon energy rises above about 1 MeV. The active marrow dose coefficients of the adult male phantom show different trends around the photon energy of 0.1 MeV because a different method was used for the calculation of active marrow dose in the adult male phantom [5]. Figure 4(b) shows the effective dose coefficients for different age phantoms in AP geometry. As expected from figure 2(a), we found small differences across the phantoms (COV 3.7%) and did not observe a clear dependency on the age of the phantoms. At the energy of 0.1 MeV, the phantoms representing older ages tend to receive greater effective dose than those representing younger ages, which may be caused by the greater contribution of back scattering to the forwardly-located organs in the older phantoms. However, the age dependency of effective dose was clearly noticed in the RLAT geometry as shown in figure 4(c), which is expected from figure 2(b).

3.3. Dependency of dose coefficients on irradiation geometry

As shown in figure 5, organ dose coefficients vary significantly for different irradiation geometries. The lungs of the newborn male phantom (figure 5(a)) show the largest dose coefficients in PA geometry (1.347 Gy/Gy at 0.1 MeV) and the smallest values in LLAT geometry (0.821 Gy/Gy at 0.1 MeV), which is similar to the value in RLAT geometry (0.836 Gy/Gy at 0.1 MeV). The lungs receive more radiation dose per unit air kerma in ROT geometry than in ISO. The colon in the newborn male phantom (figure 5(b)) shows the greatest dose coefficient in AP geometry (1.510 Gy/Gy at 0.1 MeV) with the smallest value in LLAT geometry (0.782 Gy/Gy at 0.1 MeV). Because the colon is more forwardly located compared to the lungs, the organ dose coefficients in AP geometry are much greater (up to 1.7-fold at 0.1 MeV) than those in PA geometry. The COV ranges from 18% (newborn male) to 38% (15 year old male) across irradiation geometries for the major organs (active marrow, colon, lung, stomach wall, and breast) at the energy of 0.1 MeV.

Figure 6(a) shows the dose coefficients for the active marrow of the 10 year old male phantom in different irradiation geometries. The dose coefficients in PA geometry show up to 1.6-fold greater values compared to RLAT geometry, which appear to be caused by the location of the vertebra in the back of the human body. About 30% of active marrow is included in the cervical, thoracic, lumbar vertebra, and sacrum in 10 year old child [28]. Effective dose coefficients show the greatest values in AP geometry compared to other geometries (figure 6(b)). This can be explained because the organs contributing mostly to the effective dose, i.e. colon, lung, stomach, and breast, having the highest tissue weighting factor of 0.12 [24] are located in the anterior part of the human body. The tissue weighting factor used for the colon, lung, stomach, and breast was 0.12, which contributes about 50% of the effective dose.

3.4. Uses, limitations and other considerations

In considering potential uses of organ and effective dose coefficients for children and adolescents, some limitations should be recognised. First, the dose coefficients reported here are derived from reference phantoms and, thus, most appropriately apply to representative, unidentified children or adolescents of each age, i.e., persons of reference body size and shape for each specific age. Children of the same age may vary significantly in size. Hence, there is

a significant chance for mis-specification of the phantom with the child's actual size. The use of these dose coefficients for identified individuals may result in a bias with a magnitude and direction depending on the difference in the individual subject morphometry compared to that of the reference phantom. Details on the anatomic characteristics of the pediatric phantoms can be found in the ICRP Publication 89 [28]. Second, another limitation is that in the potential use of ionising radiation in medicine, children and adolescents are rarely exposed to mono-energetic radiation in idealised geometries. Most radiation used in diagnostic examinations is based on broad radiation spectra (typically *bremsstrahlung* radiation) in more complicated exposure geometries. To incorporate radiation spectra, proper dose coefficients can be determined by integration over the entire radiation spectrum [34]. It also must be noted that usually only a portion of the body is exposed to radiation in medical radiation procedures rather than the whole body that was simulated in the current study.

The use of effective dose, particularly for children and adolescents, requires careful consideration. As stated in the ICRP Publication 103 [30], the main uses of effective dose are the prospective dose assessment for planning and optimisation in radiological protection, and demonstration of compliance with dose limits for regulatory purposes. Since most optimisation planning refers to occupational settings, there are likely few exposure scenarios for children and adolescents that would require dose coefficients for whole body idealised external exposures. In parallel, it should be realised that the tissue weighting factors [19] used here to estimate effective dose coefficients were not specifically derived for children and adolescents but represent an average over a range of ages. Furthermore, risk coefficients that might be paired with estimated effective doses for children and adolescents for estimating population detriment have also not been derived specifically for those ages. Any resulting predictions of population risk to children and adolescents are clearly uncertain for a number of reasons including those discussed here [2, 35].

4. Conclusion

We calculated a comprehensive set of organ absorbed dose (Gy/Gy) and effective dose coefficients (Sv/Gy) by coupling the ICRP reference pediatric computational phantoms with the Monte Carlo transport code. Organ dose coefficients were calculated for 28 organs and tissues including the active marrow for 10 phantoms (newborn, 1 year, 5 year, 10 year, and 15 year old male and female). Radiation exposure was simulated for 33 photon energies (0.01–20 MeV) in six idealised whole body irradiation geometries: antero-posterior (AP), postero-anterior (PA), right lateral (RLAT), left lateral (LLAT), rotational (ROT), and isotropic (ISO). The results of the present study showed that doses to the most critical organs could be significantly higher at younger ages, except for anterior-posterior irradiation, where smaller differences were observed. In this case, organ doses from AP irradiation have less variation with age than for other irradiation geometries. Because most of the major target organs are located towards the front of the body, the depth of the organs in AP geometry does not vary as much with body size as with other geometries. As expected, irradiation geometry plays an important role in the age-dependency of organ doses and subsequently on the effective dose. Our comprehensive dataset is available in tabulated form in an Excel Spreadsheet, which can be downloaded from the journal website. The data will be useful for the users who use the ICRP pediatric reference phantoms for Monte Carlo dose calculation to benchmark their calculation process.

Acknowledgments

This work was supported by the National Cancer Institute Intramural Research Program and by the Intra-Agency agreement between the National Institute of Allergy and Infectious Diseases and the National Cancer Institute, NIAID agreement Y2-Al-5077 and NCI agreement Y3-CO-5117. The authors would like to thank the members of the Task Group, Computational Phantom and Radiation Transport, of the International Commission on Radiological Protection for their invaluable comments and suggestions to develop the reference paediatric phantoms.

References

[1] Committee to Assess Health Risks from Exposure to Low Levels of Ionizing Radiation 2006 *Health Risks from Exposure to Low Levels of Ionizing Radiation* (Washington, DC: National Academies)
[2] UNSCEAR 2013 *Sources, Effects and Risks of Ionizing Radiation* United Nations
[3] ICRP 1987 Data for use in protection against external radiation *Ann. ICRP* **17** 1–132
[4] ICRP 1996 Conversion coefficients for use in radiological protection against external radiation *Ann. ICRP* **26** 1–205
[5] ICRP 2010 Conversion coefficients for radiological protection quantities for external radiation exposures *Ann. ICRP* **40** 1–258
[6] Eckerman K F, Cristy E and Ryman J C 1996 *The ORNL Mathematical Phantom Series* Oak Ridge National Laboratory
[7] Xu X G 2014 An exponential growth of computational phantom research in radiation protection, imaging, and radiotherapy: a review of the fifty-year history *Phys. Med. Biol.* **59** R233–302
[8] Caon M 2004 Voxel-based computational models of real human anatomy: a review *Radiat. Environ. Biophys.* **42** 229–35
[9] ICRP 2009 Adult reference computational phantoms *Ann. ICRP* **39** 1–166
[10] ICRP 1973 Data for protection against ionizing from external sources—supplement to ICRP publication 15 *Ann. ICRP* **21** 1–101
[11] Yamaguchi Y 1994 Age-dependent effective doses for external photons *Radiat. Prot. Dosim.* **55** 123–9
[12] Yamaguchi Y 1994 Age-dependant effective doses for neutrons from thermal to 18.3 MeV *Radiat. Prot. Dosim.* **55** 257–63
[13] Chou D P, Wang J N and Chen I J 2001 Age-dependent protection quantities for external photon irradiation *Radiat. Prot. Dosim.* **95** 215–23
[14] Chou D P, Wang J N, Chen I J and Chang B J 2003 Age-dependent protection quantities for external neutron irradiation *Radiat. Prot. Dosim.* **104** 5–16
[15] Zankl M, Veit R, Williams G, Schneider K, Fendel H, Petoussi N and Drexler G 1988 The construction of computer tomographic phantoms and their application in radiology and radiation protection *Radiat. Environ. Biophys.* **27** 153–64
[16] Zankl M, Petoussi-Henss N, Fill U and Regulla D 2003 The application of voxel phantoms to the internal dosimetry of radionuclides *Radiat. Prot. Dosim.* **105** 539–48
[17] Petoussi N, Jacob P, Zankl M and Saito K 1991 Organ doses for fetuses, babies, children and adults from environmental gamma-rays *Radiat. Prot. Dosim.* **37** 31–41
[18] Petoussi-Henss N, Schlattl H, Zankl M, Endo A and Saito K 2012 Organ doses from environmental exposures calculated using voxel phantoms of adults and children *Phys. Med. Biol.* **57** 5679–713
[19] Zankl M, Fill U, Petoussi-Henss N and Regulla D 2002 Organ dose conversion coefficients for external photon irradiation of male and female voxel models *Phys. Med. Biol.* **47** 2367–85
[20] Zankl M, Panzer W and Drexler G 1992 The calculation of organ doses from computed-tomography examinations *Radiat. Prot. Dosim.* **43** 237–9
[21] Zankl M, Panzer W, Petoussi-Henss N and Drexler G 1995 Organ doses for children from computed tomographic examinations *Radiat. Prot. Dosim.* **57** 393–6
[22] Veit R and Zankl M 1993 Variation of organ doses in pediatric radiology due to patient diameter, calculated with phantoms of varying voxel size *Radiat. Prot. Dosim.* **49** 353–6

[23] Zankl M, Panzer W and Herrmann C 2000 Calculation of patient doses using a human voxel phantom of variable diameter *Radiat. Prot. Dosim.* **90** 155–8
[24] Caon M, Bibbo G and Pattison J 1997 A comparison of radiation dose measured in CT dosimetry phantoms with calculations using EGS4 and voxel-based computational models *Phys. Med. Biol.* **42** 219–29
[25] Lee C, Lee C and Bolch W E 2006 Age-dependent organ and effective dose coefficients for external photons: a comparison of stylized and voxel-based paediatric phantoms *Phys. Med. Biol.* **51** 4663–88
[26] Lee C, Lee C, Williams J L and Bolch W E 2006 Whole-body voxel phantoms of paediatric patients—UF series B *Phys. Med. Biol.* **51** 4649–61
[27] Lee C, Lodwick D, Hurtado J, Pafundi D, Williams J L and Bolch W E 2010 The UF family of reference hybrid phantoms for computational radiation dosimetry *Phys. Med. Biol.* **55** 339–63
[28] ICRP 2002 Basic anatomical and physiological data for use in radiological protection: reference values *Ann. ICRP* **32** 1–277
[29] ICRU 1992 *Photon, Electron, Proton and Neutron Interaction Data for Body Tissues* vol 46 (Bethesda, MD: International Commission on Radiation Units and Measurements)
[30] ICRP 2007 The 2007 recommendations of the International Commission on Radiological Protection *Ann. ICRP* **37** 1–332
[31] Pelowitz D B 2011 *MCNPX User's Manual Version 2.7.0* Los Alamos National Laboratory
[32] Cristy M and Eckerman K F 1987 *Specific Absorbed Fractions of Energy at Various Ages from Internal Photon Sources* (Oak Ridge, TN: Oak Ridge National Laboratory)
[33] Johnson P B, Bahadori A A, Eckerman K F, Lee C and Bolch W E 2011 Response functions for computing absorbed dose to skeletal tissues from photon irradiation—an update *Phys. Med. Biol.* **56** 2347
[34] Simon S L 2011 Organ-specific external dose coefficients and protective apron transmission factors for historical dose reconstruction for medical personnel *Health Phys.* **101** 13–27
[35] Hendee W R 2013 International organization for medical physics policy statement of the international organization for medical physics *Radiology* **267** 326–7